

## Thermal-hydro-mechanical coupling stress intensity factor of brittle rock

Peng LI<sup>1</sup>, Qiu-hua RAO<sup>1</sup>, Zhuo LI<sup>1</sup>, Jing JING<sup>2</sup>

1. School of Civil Engineering, Central South University, Changsha 410075, China;

2. School of Resources and Safety Engineering, Central South University, Changsha 410083, China

Received 30 October 2013; accepted 19 January 2014

**Abstract:** A new calculation formula of THM coupling stress intensity factor was derived by the boundary collocation method, in which an additional constant stress function was successfully introduced for the cracked specimen with hydraulic pressure applied on its crack surface. Based on the newly derived formula, THM coupling fracture modes (including tensile, shear and mixed fracture mode) can be predicted by a new fracture criterion of stress intensity factor ratio, where the maximum axial load was measured by self-designed THM coupling fracture test. SEM analyses of THM coupling fractured surface indicate that the higher the temperature and hydraulic pressure are and the lower the confining pressure is, the more easily the intergranular (tension) fracture occurs. The transgranular (shear) fracture occurs in the opposite case while the mixed-mode fracture occurs in the middle case. The tested THM coupling fracture mechanisms are in good agreement with the predicted THM coupling fracture modes, which can verify correction of the newly-derived THM coupling stress intensity factor formula.

**Key words:** stress intensity factor; thermal-hydro-mechanical coupling; boundary collocation method; fracture mechanism; brittle rock

### 1 Introduction

In deep exploitation of minerals and oil, geothermal development, nuclear waste disposal and underground energy storage, brittle rock is usually subjected to thermal-hydro-mechanical (THM) coupling condition and THM coupling fracture easily occurs, which attracts more and more attentions of researcher [1–3]. It is very important to calculate stress intensity factor for determining fracture mode in study of THM coupling fracture [4,5]. Currently, available literatures of coupling stress intensity factor calculation are only focused on thermal-mechanical (TM) or hydro-mechanical (HM) coupling condition. For example, weight function method [6,7] and interaction integral method [8] were used to deduce TM coupling stress intensity factors of the semi-elliptical crack, circumferential crack and three dimensional curved crack. Scaled boundary finite element method [9], Geertsma's model method [10] and superposition principle method [11,12] were applied to calculating HM coupling stress intensity factors of the

opening crack and compressive-shear crack. Although there are very few literatures on the simulation of THM coupling fracture process by using virtual multi-dimensional internal bonds method [13] and hybrid finite difference-displacement discontinuity method [14], there is lacking in study of THM coupling stress intensity factor.

In this study, the traditional boundary collocation was used to deduce THM coupling stress intensity factor formula by firstly introducing an additional constant stress function, since this method was only suitable for calculating stress intensity factor of the cracked specimen without any force on its crack surface. THM coupling fracture mode (including tensile, shear and mixed mode fracture) could be predicted by a new criterion of stress intensity factor ratio and self-designed THM coupling fracture test. THM coupling fracture mechanism was revealed by analyzing microscopic characteristics of fractured surface and compared with the predicted THM coupling fracture mode in order to verify the newly-derived THM coupling stress intensity factor formula.

## 2 Derivation of THM coupling stress intensity factor

### 2.1 Calculation model

A standard cylinder specimen ( $D=50$  mm,  $L=100$  mm) was adopted (Fig. 1), with an inclined penetrating crack of  $2a=30$  mm and  $\alpha=45^\circ$  and subjected to THM coupling condition (i.e., temperature  $t$ , hydraulic pressure  $p_H$ , confining pressure  $p_M$  and axial pressure  $p_L$ ). Table 1 shows different THM coupling conditions for calculation, where the axial pressure was unit pressure ( $p_L=1$  MPa) and the hydraulic pressure ( $p_H$ ) must be smaller than the confining pressure ( $p_M$ ) in order to avoid the mixture of water and oil. The temperature must be controlled within  $100$  °C for preventing evaporation of water, since actual temperature in deep mining is lower than  $100$  °C.  $\Delta t$ ,  $\alpha$ , and  $E_T$  were temperature difference between room temperature and tested temperature, thermal expansion

coefficient and elastic modulus, respectively.

### 2.2 Formula derivation

#### 2.2.1 Stress function

As shown in Fig. 1, a global rectangular coordinate system ( $XOY$ ) was set at the center of crack surface ( $O$ ), and a local rectangular ( $xoy$ ) and a polar ( $ox$ ) coordinate systems were set at the crack tip ( $o$ ).

The boundary collocation method was applied to calculating stress intensity factor of the cylinder specimen under THM coupling condition, where a biharmonic stress function must be chosen appropriately to meet all boundary conditions. Generally, the stress function ( $\varphi_1$ ) is in the form of series expansion only for the crack without applied force on its surface. For the THM coupling specimen with the hydraulic pressure  $p_H$  (Fig. 1), it is necessary to introduce an additional constant stress function ( $\varphi_2$ ). The stress function  $\varphi$  is written as the sum of  $\varphi_1$  and  $\varphi_2$ .

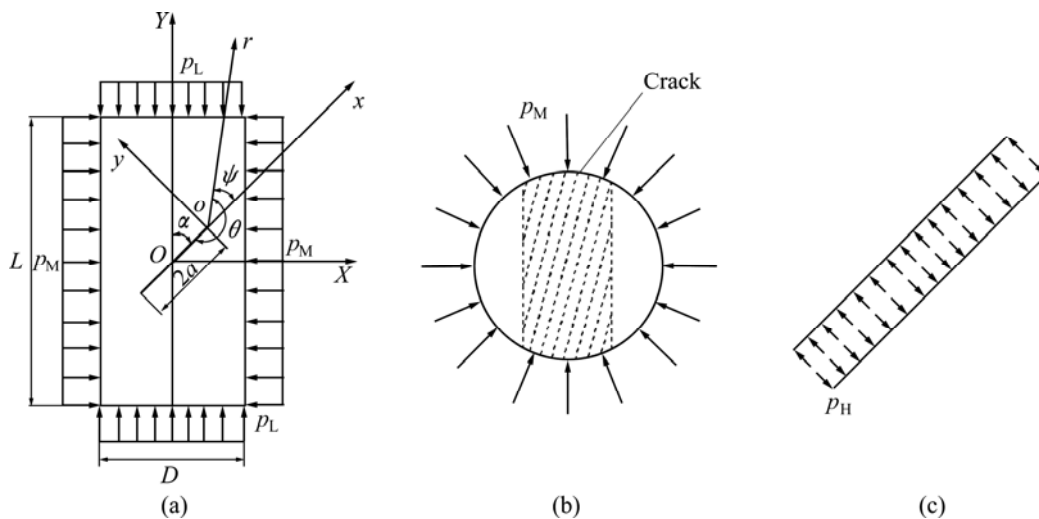


Fig. 1 THM coupling calculation model: (a) Front view; (b) Top view; (c) Enlarged crack surface

Table 1 THM coupling loading condition

No.	$t/^\circ\text{C}$	$\Delta t/^\circ\text{C}$	$\alpha/^\circ\text{C}$	$E_T/\text{GPa}$	$p_L/\text{MPa}$	$p_H/\text{MPa}$	$p_M/\text{MPa}$
T1	25	0	$5 \times 10^{-6}$	10.67	1	2	4
T2	50	25	$5 \times 10^{-6}$	10.54	1	2	4
T3	70	45	$5 \times 10^{-6}$	10.50	1	2	4
T4	90	65	$5 \times 10^{-6}$	10.48	1	2	4
H1	70	45	$5 \times 10^{-6}$	10.50	1	1.5	4
H2	70	45	$5 \times 10^{-6}$	10.50	1	2.5	4
H3	70	45	$5 \times 10^{-6}$	10.50	1	3.5	4
M1	50	25	$5 \times 10^{-6}$	10.54	1	2	2.5
M2	50	25	$5 \times 10^{-6}$	10.54	1	2	3
M3	50	25	$5 \times 10^{-6}$	10.54	1	2	4.5

$$\varphi_1 = \sum_{n=1}^{\infty} r^{\frac{n}{2}+1} \left[ A_n \sin\left(\frac{n}{2}+1\right)\theta + B_n \cos\left(\frac{n}{2}+1\right)\theta + C_n \sin\left(\frac{n}{2}-1\right)\theta + D_n \cos\left(\frac{n}{2}-1\right)\theta \right] = \sum_{n=1}^{\infty} r^{\frac{n}{2}+1} F(\theta) \tag{1}$$

$$\varphi_2 = -p_H \frac{r^2}{2} \tag{2}$$

$$\varphi = \varphi_1 + \varphi_2 \tag{3}$$

where  $A_n, B_n, C_n,$  and  $D_n$  are coefficients determined by boundary conditions. Obviously, the stress function  $\varphi$  can satisfy the biharmonic equation  $\nabla^2 \nabla^2 \varphi = 0$ .

In the polar coordinate system, the stress components are expressed as

$$\left\{ \begin{aligned} \sigma_r &= \frac{1}{r^2} \frac{\partial^2 \varphi}{\partial \theta^2} + \frac{1}{r} \frac{\partial \varphi}{\partial r} = r^{\left(\frac{n}{2}-1\right)} \left[ F''(\theta) + \left(\frac{n}{2}+1\right) F(\theta) \right] - p_H \\ \sigma_\theta &= \frac{\partial^2 \varphi}{\partial r^2} = r^{\left(\frac{n}{2}-1\right)} \frac{n}{2} \left(\frac{n}{2}+1\right) F(\theta) - p_H \\ \tau_{r\theta} &= \frac{1}{r^2} \frac{\partial \varphi}{\partial \theta} - \frac{1}{r} \frac{\partial^2 \varphi}{\partial r \partial \theta} = -r^{\left(\frac{n}{2}-1\right)} \frac{n}{2} F'(\theta) \end{aligned} \right. \tag{4}$$

Substituting the boundary condition of crack surface (when  $\theta=0, \sigma_\theta=-p_H$  and  $\tau_{r\theta}=0$ ) into Eq. (4), it becomes

$$B_n + D_n = 0$$

$$\left(\frac{n}{2}+1\right)A_n + \left(\frac{n}{2}-1\right)C_n = 0$$

i.e.,

$$B_n = -D_n$$

$$A_n = -\frac{n-2}{n+2} C_n$$

Therefore, the stress function is simplified as

$$\varphi(r, \theta) = \sum_{n=1}^{\infty} r^{\frac{n}{2}+1} \left\{ C_n \left[ \sin\left(\frac{n}{2}-1\right)\theta - \frac{n-2}{n+2} \sin\left(\frac{n}{2}+1\right)\theta \right] + D_n \left[ \cos\left(\frac{n}{2}-1\right)\theta - \cos\left(\frac{n}{2}+1\right)\theta \right] \right\} - p_H \frac{r^2}{2} \tag{5}$$

In order to determine the coefficients  $A_n, B_n, C_n,$  and  $D_n$  conveniently, angle  $\psi$  is introduced and positive angle  $\psi$  is defined in anticlockwise direction (Fig. 1(a)). Substitute  $\psi = \theta - \pi$  into Eq. (5) and then rewrite the

stress function  $\varphi$  in the sum of even function  $\varphi_e(r, \psi)$  and odd function  $\varphi_o(r, \psi)$  for calculating tensile (Mode I) and shear (Mode II) stress intensity factor, respectively.

$$\varphi(r, \psi) = \varphi_e(r, \psi) + \varphi_o(r, \psi) \tag{6}$$

$$\begin{aligned} \varphi_e(r, \psi) &= \sum_{m=1}^{\infty} (-1)^{m-1} a_{2m-1} r^{m+\frac{1}{2}} \times \\ &\left[ \frac{2m-3}{2m+1} \cos\left(m+\frac{1}{2}\right)\psi - \cos\left(m-\frac{3}{2}\right)\psi \right] + \\ &\sum_{m=1}^{\infty} (-1)^m a_{2m} r^{m+1} \times \left[ \cos(m+1)\psi - \cos(m-1)\psi \right] - p_H \frac{r^2}{2} \end{aligned} \tag{7}$$

$$\begin{aligned} \varphi_o(r, \psi) &= \sum_{m=1}^{\infty} (-1)^{m-1} b_{2m-1} r^{m+\frac{1}{2}} - \\ &\left[ \sin\left(m-\frac{3}{2}\right)\psi - \sin\left(m+\frac{1}{2}\right)\psi \right] + \\ &\sum_{m=1}^{\infty} (-1)^m b_{2m} r^{m+1} \left[ \frac{m-1}{m+1} \sin(m+1)\psi - \sin(m-1)\psi \right] \end{aligned} \tag{8}$$

Since the stress intensity factor at crack tip is calculated when  $r \rightarrow 0$ , only the least power term  $r^{3/2}$  in Eqs. (7) and (8) needs to be considered and thus Eq. (6) becomes

$$\begin{aligned} \varphi(r, \psi) &= a_1 r^{\frac{3}{2}} \left( -\cos\frac{1}{2}\psi - \frac{1}{3} \cos\frac{3}{2}\psi \right) + \\ &b_1 r^{\frac{3}{2}} \left( -\sin\frac{1}{2}\psi - \sin\frac{3}{2}\psi \right) \end{aligned} \tag{9}$$

The stress components in the polar coordinate system can be obtained by substituting Eq. (9) into Eq. (4)

$$\left\{ \begin{aligned} \sigma_r &= \frac{a_1}{4\sqrt{r}} \left( -5 \cos\frac{1}{2}\psi + \cos\frac{3}{2}\psi \right) + \\ &\frac{b_1}{4\sqrt{r}} \left( -5 \sin\frac{\psi}{2} + 3 \sin\frac{3}{2}\psi \right) \\ \sigma_\psi &= -\frac{a_1}{4\sqrt{r}} \left( -3 \cos\frac{1}{2}\psi - \cos\frac{3}{2}\psi \right) + \\ &\frac{b_1}{4\sqrt{r}} \left( -3 \sin\frac{\psi}{2} - 3 \sin\frac{3}{2}\psi \right) \\ \tau_{r\psi} &= \frac{a_1}{4\sqrt{r}} \left( -\sin\frac{\psi}{2} - \sin\frac{3}{2}\psi \right) + \\ &\frac{b_1}{4\sqrt{r}} \left( \cos\frac{\psi}{2} + 3 \cos\frac{3}{2}\psi \right) \end{aligned} \right. \tag{10}$$

and the stress components in rectangular coordinate system can be obtained by coordinate transformation.

$$\left\{ \begin{aligned} \sigma_x &= -\frac{a_1\sqrt{2\pi}}{\sqrt{2\pi r}} \cos \frac{\psi}{2} \left(1 - \sin \frac{\psi}{2} \sin \frac{3\psi}{2}\right) - \\ &\quad \frac{b_1\sqrt{2\pi}}{\sqrt{2\pi r}} \sin \frac{\psi}{2} \left(2 + \cos \frac{\psi}{2} \cos \frac{3\psi}{2}\right) \\ \sigma_y &= -\frac{a_1\sqrt{2\pi}}{\sqrt{2\pi r}} \cos \frac{\psi}{2} \left(1 + \sin \frac{\psi}{2} \cos \frac{3\psi}{2}\right) + \\ &\quad \frac{b_1\sqrt{2\pi}}{\sqrt{2\pi r}} \sin \frac{\psi}{2} \cos \frac{\psi}{2} \cos \frac{3\psi}{2} \\ \tau_{xy} &= -\frac{a_1\sqrt{2\pi}}{\sqrt{2\pi r}} \cos \frac{\psi}{2} \sin \frac{\psi}{2} \cos \frac{3\psi}{2} + \\ &\quad \frac{b_1\sqrt{2\pi}}{\sqrt{2\pi r}} \cos \frac{\psi}{2} \left(1 - \sin \frac{\psi}{2} \sin \frac{3\psi}{2}\right) \end{aligned} \right. \quad (11)$$

According to the stress components under mixed mode loading

$$\left\{ \begin{aligned} \sigma_x &= \frac{K_I}{\sqrt{2\pi r}} \cos \frac{\psi}{2} \left(1 - \sin \frac{\psi}{2} \sin \frac{3\psi}{2}\right) - \\ &\quad \frac{K_{II}}{\sqrt{2\pi r}} \sin \frac{\psi}{2} \left(2 + \cos \frac{\psi}{2} \cos \frac{3\psi}{2}\right) \\ \sigma_y &= \frac{K_I}{\sqrt{2\pi r}} \cos \frac{\psi}{2} \left(1 + \sin \frac{\psi}{2} \cos \frac{3\psi}{2}\right) + \\ &\quad \frac{K_{II}}{\sqrt{2\pi r}} \sin \frac{\psi}{2} \cos \frac{\psi}{2} \cos \frac{3\psi}{2} \\ \tau_{xy} &= \frac{K_I}{\sqrt{2\pi r}} \cos \frac{\psi}{2} \sin \frac{\psi}{2} \cos \frac{3\psi}{2} + \\ &\quad \frac{K_{II}}{\sqrt{2\pi r}} \cos \frac{\psi}{2} \left(1 - \sin \frac{\psi}{2} \sin \frac{3\psi}{2}\right) \end{aligned} \right. \quad (12)$$

Modes I and II stress intensity factors  $K_I$  and  $K_{II}$  can be calculated by comparing Eqs. (11) and (12) as follows.

$$\left\{ \begin{aligned} K_I &= -a_1\sqrt{2\pi} \\ K_{II} &= b_1\sqrt{2\pi} \end{aligned} \right. \quad (13)$$

It is seen that  $K_I$  and  $K_{II}$  depend only on the two coefficients  $a_1$  and  $b_1$ . The two coefficients can be determined by boundary conditions, i.e., selecting several points at the boundary except the crack surface (which is included in the stress function  $\varphi_2$ ) and solving the equations of  $a_1$  and  $b_1$  established by the boundary condition.

2.2.2 Coefficients for stress function

For different values of  $m$  ( $m=1, 2, \dots$ ) in Eqs. (6–8), there are different numbers of the coefficients  $a$  and  $b$ , and different numbers of the boundary points are needed for determining the different coefficients. As shown in Fig. 2, several boundary points  $M_i$  and  $N_i$  ( $i=1, 2, \dots$ ) are selected on the cylindrical generatrix passing through the crack midpoint at interval of 5 mm and their polar coordinates can be calculated by geometrical relations of the triangles (Table 2). Since any boundary point  $M_i$  or  $N_i$

( $i=1, 2, \dots$ ) has the following stress components in  $X$  and  $Y$  directions according to THM loading condition:

$$\begin{cases} \sigma_X = -p_M + \alpha E_T \Delta T \\ \sigma_Y = -p_L + \alpha E_T \Delta T \end{cases} \quad (14)$$

the coefficients  $a$  and  $b$  for the stress function can be determined by using stress analysis of the element (Fig. 3) and Eq. (4).

Table 2 Polar coordinate of boundary points

Point	$r/\text{mm}$	$\beta_i/(\circ)$	$\psi/(\circ)$	Point	$r/\text{mm}$	$\beta_2/(\circ)$	$\psi/(\circ)$
$M_1$	40.798	15.066	60.066	$N_1$	61.526	9.925	215.075
$M_2$	35.994	17.136	62.136	$N_2$	56.608	10.798	214.202
$M_3$	31.251	19.838	64.838	$N_3$	51.705	11.836	213.164
$M_4$	26.602	23.494	68.494	$N_4$	46.823	13.091	211.909
$M_5$	22.107	28.667	73.667	$N_5$	41.968	14.637	210.363
$M_6$	17.882	36.375	81.375	$N_6$	37.152	16.586	208.414
$\vdots$	$\vdots$	$\vdots$	$\vdots$	$\vdots$	$\vdots$	$\vdots$	$\vdots$

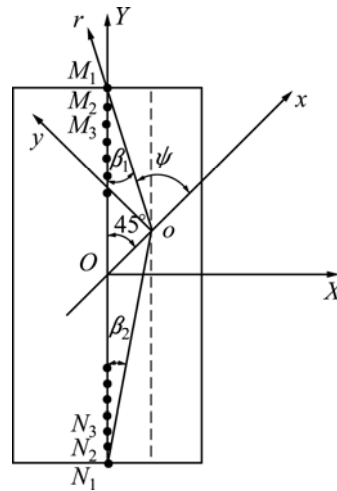


Fig. 2 Boundary points position

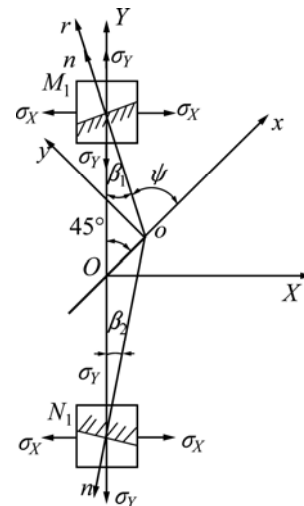


Fig. 3 Polar stress of boundary points



unchanged and can be regarded as convergence when  $m \geq 15$ . Therefore, the values of  $a_1$  and  $b_1$  in the case of  $m=15$  can meet accuracy requirements for calculating  $K_I$  and  $K_{II}$ .

### 2.2.3 Stress intensity factor

For the specimen T1 under THM coupling condition, modes I and II stress intensity factors are calculated by substituting the values of  $a_1$  and  $b_1$  ( $m=15$ ) into Eq. (13).

$$\begin{cases} K_I = 0.025 \text{ MPa} \cdot \text{m}^{1/2} \\ K_{II} = 0.083 \text{ MPa} \cdot \text{m}^{1/2} \end{cases} \quad (21)$$

Table 4 lists the stress intensity factors of different specimens with different THM coupling conditions (Table 1). Calculation formulae of THM coupling stress intensity factors can be obtained by fitting method.

$$\begin{cases} K_I = \frac{p_L p_H t a \sqrt{a} \cos \alpha}{2\sqrt{2} D p_M t_0} \left[ 136.11 \left( \frac{a}{D} \right)^3 + 247.164 \left( \frac{a}{D} \right)^4 + 0.001 \right] \\ K_{II} = \frac{p_L t a \sqrt{a} \sin \alpha}{2\sqrt{2} D t_0} \left[ 147.234 \left( \frac{a}{D} \right)^3 + 126.504 \left( \frac{a}{D} \right)^4 + 0.235 \right] \end{cases} \quad (22)$$

**Table 4** THM coupling stress intensity factors

No.	$K_I / (\text{MPa} \cdot \text{m}^{1/2})$	$K_{II} / (\text{MPa} \cdot \text{m}^{1/2})$
T1	0.025	0.083
T2	0.049	0.100
T3	0.073	0.118
T4	0.106	0.144
H1	0.058	0.144
H2	0.093	0.142
H3	0.131	0.155
M1	0.114	0.123
M2	0.073	0.119
M3	0.042	0.106

## 3 Test verification

### 3.1 Test arrangement

Rock material was local red sandstone, and its mineral composition was quartz (90.0%) and little feldspar (4.1%) cemented by hydromica (4.8%) and kaolinite (1.1%), etc. Rock specimen was the same as the calculation model (Fig. 1), i.e., standard cylinder of  $d50 \text{ mm} \times 100 \text{ mm}$  with a penetrating precrack of  $2a=30 \text{ mm}$  and  $\alpha=45^\circ$ . An additional vertical hole of  $d3 \text{ mm} \times 50 \text{ mm}$  was drilled from the bottom center of the specimen to the crack surface in order to apply the hydraulic pressure  $P_H$  on the crack surface (Fig. 4).

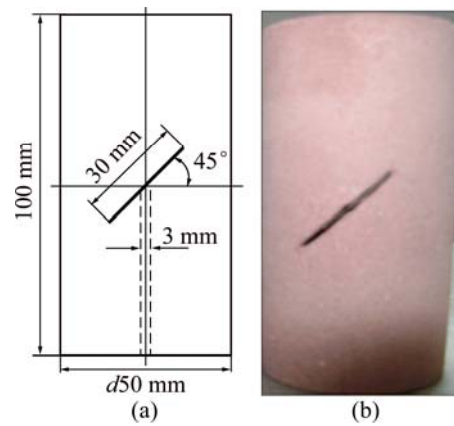


**Fig. 4** Rock specimen: (a) Model; (b) Real object

THM coupling fracture test was conducted by the self-designed THM coupling testing system (Fig. 5), including tri-axial loading system, hydraulic pressure and confining pressure loading system. The hydraulic pressure and confining pressure system were connected to the tri-axial loading system by high-strength hose, in which special isolation films were used to avoid the water mixing with the oil. Before the test, both the rock specimen and the water were heated to the specific temperature  $t$ . The temperature  $t$  must be controlled within  $100^\circ \text{C}$  for preventing evaporation of water since actual temperature in deep mining is lower than  $100^\circ \text{C}$ .

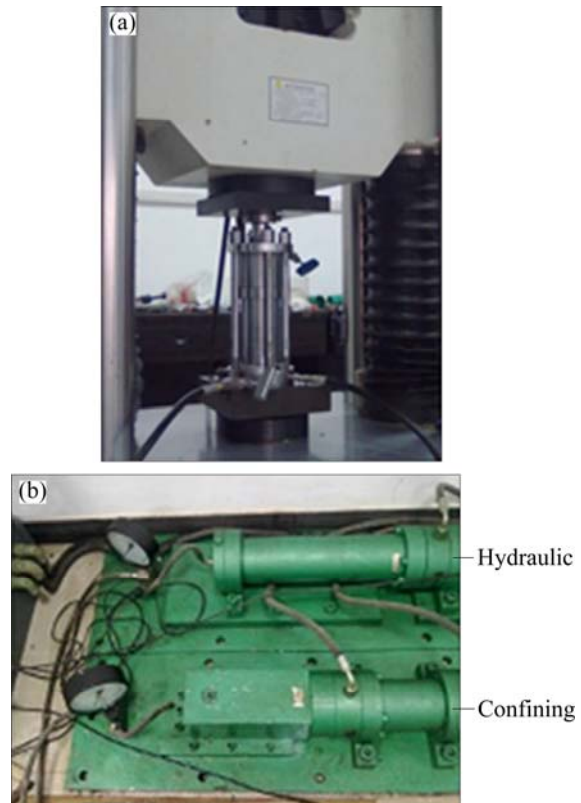


**Fig. 5** THM coupling testing system: (a) Tri-axial loading system; (b) Hydraulic and confining pressure system

and the hydraulic pressure  $p_H$  must be smaller than the confining pressure  $p_M$  in order to prevent the water mixing with oil, as shown in Table 1. During the test, the maximum axial pressure  $p_{L,max}$  was recorded for calculating the maximum stress intensity factors  $K_{I,max}$  and  $K_{II,max}$  (Eq. (22)) and microscopic characteristics of the fractured specimens were analyzed by a scanning electron microscope for revealing the fracture mechanism.

**3.2 Test results and analysis**

**3.2.1 Fracture mode**

In classical fracture mechanics, fracture mode (Mode I or Mode II) is assumed to be the same as loading forms (tension or shear). That is suitable for most metal materials. For brittle rock with much smaller tensile strength than shear strength, the shear loading results in the tensile fracture rather than the shear fracture. Therefore, a new fracture criterion of stress intensity factor ratio has been established based on the fact that the fracture mode ( Mode I, II or mixed mode) depends on the ratio of maximum shear to tensile stress intensity factor at crack tip ( $K_{II,max}/K_{I,max}$ ) but not the loading mode as follows [15].

$$\begin{cases} \frac{K_{II,max}}{K_{I,max}} < \frac{K_{IIC}}{K_{IC}} \text{ and } K_{I,max} = K_{IC}, \text{ Mode I} \\ \frac{K_{II,max}}{K_{I,max}} > \frac{K_{IIC}}{K_{IC}} \text{ and } K_{II,max} = K_{IIC}, \text{ Mode II} \\ \frac{K_{II,max}}{K_{I,max}} = \frac{K_{IIC}}{K_{IC}} \text{ and } K_{I,max} = K_{IC}, K_{II,max} = K_{IIC}, \\ \text{mixed mode} \end{cases} \quad (23)$$

In the new fracture criterion, the maximum modes I and II stress intensity factors ( $K_{I,max}$  and  $K_{II,max}$ ) of the THM coupling specimens are calculated by substituting the tested value of maximum axial pressure  $p_{L,max}$  (Table 5) into Eq. (22). Modes I and II fracture toughness ( $K_{IC}$  and  $K_{IIC}$ ) of the red sandstone were obtained by three-points bending test and shear-box test at different

temperatures  $t$  (Table 5), since  $K_{IC}$  and  $K_{IIC}$  (as a material constant) are independent of the hydraulic pressure  $p_H$ , confining pressure  $p_M$  and axial pressure  $p_L$ , but affected by temperature  $t$ . Thus the fracture modes of the THM coupling specimens can be predicted (Table 5) according to the new fracture criterion (Eq. (23)).

**3.2.2 Fracture trajectory and fracture mechanism**

Figures 6–11 show the fracture trajectories and SEM images of the THM coupling specimens, and the microscopic fracture mechanism is analyzed as follows.

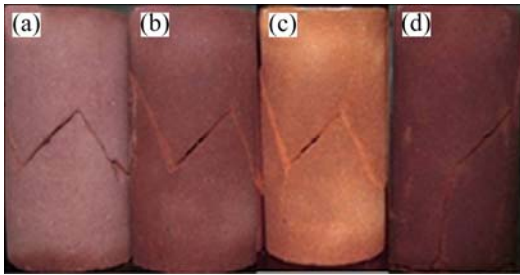
1) Under lower temperatures (Specimens T1, T2), lower hydraulic pressure (Specimen H1) and higher confining pressure (Specimen M3), the specimens have similar macroscopic and microscopic fracture characteristics (Figs. 6(a), 6(b), 7(a) and 8(d)). The cracks are initiated at the two crack tips and propagated only in one direction of negative angle ( $\psi < 0$  clockwise, Fig. 1(a)). There are many sliding steps and dense parallel stripes appearing on the fractured surfaces and transgranular fracture occurs, which are typical characteristics of Mode II (shear) fracture.

2) Under higher temperature (Specimen T4), higher hydraulic pressure (Specimen H3) and lower confining pressure (Specimen M1), the specimens have similar macroscopic and microscopic fracture characteristics (Figs. 6(d), 7(d) and 8(a)). The cracks are initiated at the two crack tips and propagated only in one direction of positive angle ( $\psi > 0$  anticlockwise, Fig. 1(a)). There are many complete crystal particles in sugar shape appearing on the fractured surfaces and intergranular fracture occurs, which are typical characteristics of Mode I (tensile) fracture.

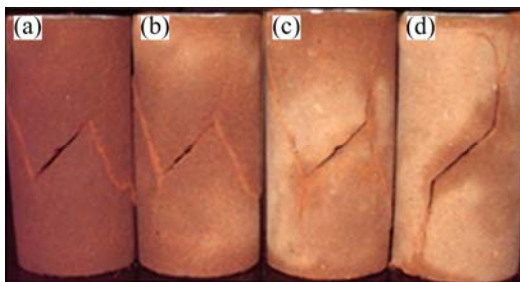
3) Under middle temperature (Specimen T3), middle hydraulic pressure (Specimen H2) and middle confining pressure (Specimen M2), the specimens have similar macroscopic and microscopic fracture characteristics (Figs. 6(c), 7(c) and 8(b)). The cracks are initiated at the two crack tips and propagated in two directions ( $\psi < 0$  clockwise and  $\psi > 0$  anticlockwise,

**Table 5** THM coupling fracture mode and mechanism of red sandstone specimens

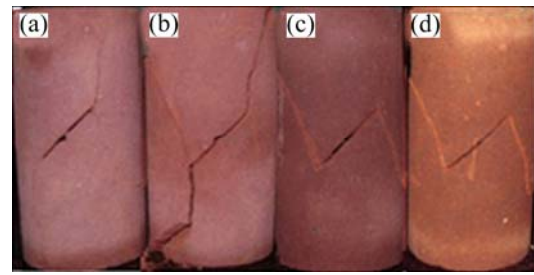
No.	$p_{L,max}/$ MPa	$K_{I,max}/$ (MPa·m <sup>1/2</sup> )	$K_{II,max}/$ (MPa·m <sup>1/2</sup> )	$K_{II,max}/$ $K_{I,max}$	$K_{IC}/$ (MPa·m <sup>1/2</sup> )	$K_{IIC}/$ (MPa·m <sup>1/2</sup> )	$K_{IIC}/$ $K_{IC}$	Predicted fracture mode	Tested fracture mechanism
T1	15.2	0.38	1.21	3.32	0.60	1.21	2.02	Shear	Shear
T2	12.8	0.63	1.28	2.03	0.75	1.25	1.67	Shear	Shear
T3	11.2	0.82	1.32	1.61	0.84	1.29	1.54	Mixed	Mixed
T4	9.3	0.99	1.34	1.35	0.91	1.36	1.49	Tension	Tension
H1	9.1	0.53	1.31	2.47	0.84	1.29	1.54	Shear	Shear
H2	9.5	0.88	1.35	1.53	0.84	1.29	1.54	Mixed	Mixed
H3	6.5	0.85	1.01	1.19	0.84	1.29	1.54	Tension	Tension
M1	6.9	0.79	0.85	1.08	0.75	1.25	1.67	Tension	Tension
M2	11.3	0.82	1.35	1.65	0.75	1.25	1.67	Mixed	Mixed
M3	11.4	0.48	1.21	2.52	0.75	1.25	1.67	Shear	Shear



**Fig. 6** Fracture trajectories of red sandstone at different temperatures: (a) Specimen T1 ( $\psi < 0$ ); (b) Specimen T2 ( $\psi < 0$ ); (c) Specimen T3 ( $\psi < 0$  and  $\psi > 0$ ); (d) Specimen T4 ( $\psi > 0$ )



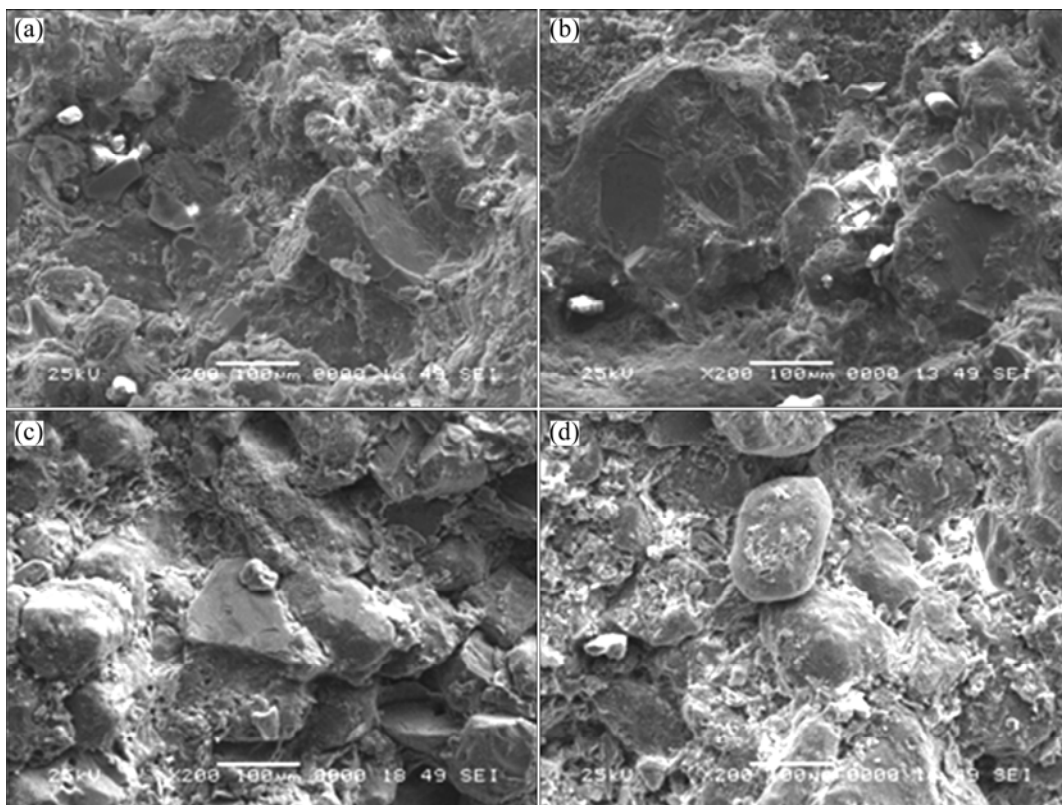
**Fig. 7** Fracture trajectories of red sandstone at different hydraulic pressures: (a) Specimen H1 ( $\psi < 0$ ); (b) Specimen T3 ( $\psi < 0$  and  $\psi > 0$ ); (c) Specimen H2 ( $\psi < 0$  and  $\psi > 0$ ); (d) Specimen H3 ( $\psi > 0$ )



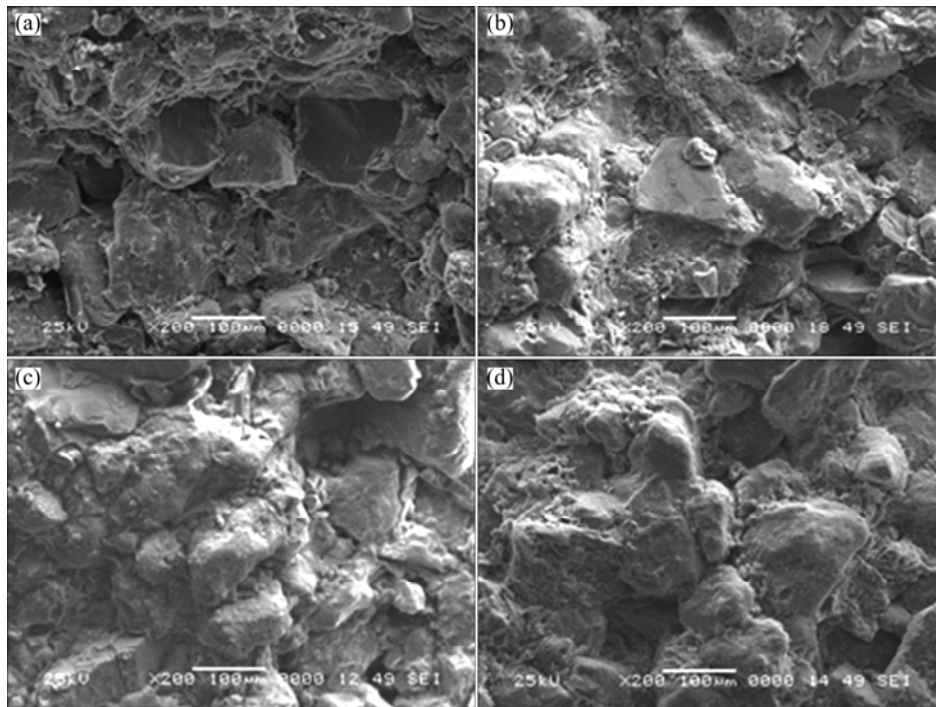
**Fig. 8** Fracture trajectories of red sandstone at different confining pressures: (a) Specimen M1 ( $\psi > 0$ ); (b) Specimen M2 ( $\psi < 0$  and  $\psi > 0$ ); (c) Specimen T2 ( $\psi < 0$ ); (d) Specimen M3 ( $\psi < 0$ )

Fig. 1(a)). Both the sliding steps of parallel stripes and the complete crystal particles in sugar shape appear on the fractured surfaces, and both the transgranular and intergranular fractures occur, which are typical characteristics of mixed mode fracture.

Table 5 lists the test results of fracture mechanisms of the THM coupling specimens based on the fracture trajectories and microscopic characteristics, which are in good agreement with the predicted results of fracture modes based on Eqs. (22) and (23). It is verified that the established calculation formula of stress intensity factor (Eq. (22)) is correct for the THM coupling specimen.



**Fig. 9** Fracture morphologies of red sandstone at different temperatures: (a) Specimen T1 (transgranular fracture); (b) Specimen T2 (transgranular fracture); (c) Specimen T3 (transgranular and intergranular fracture); (d) Specimen T4 (intergranular fracture)



**Fig. 10** Fracture morphologies of red sandstone at different hydraulic pressures: (a) Specimen H1 (transgranular fracture); (b) Specimen T3 (transgranular and intergranular fracture); (c) Specimen H2 (transgranular and intergranular fracture); (d) Specimen H3 (intergranular fracture)

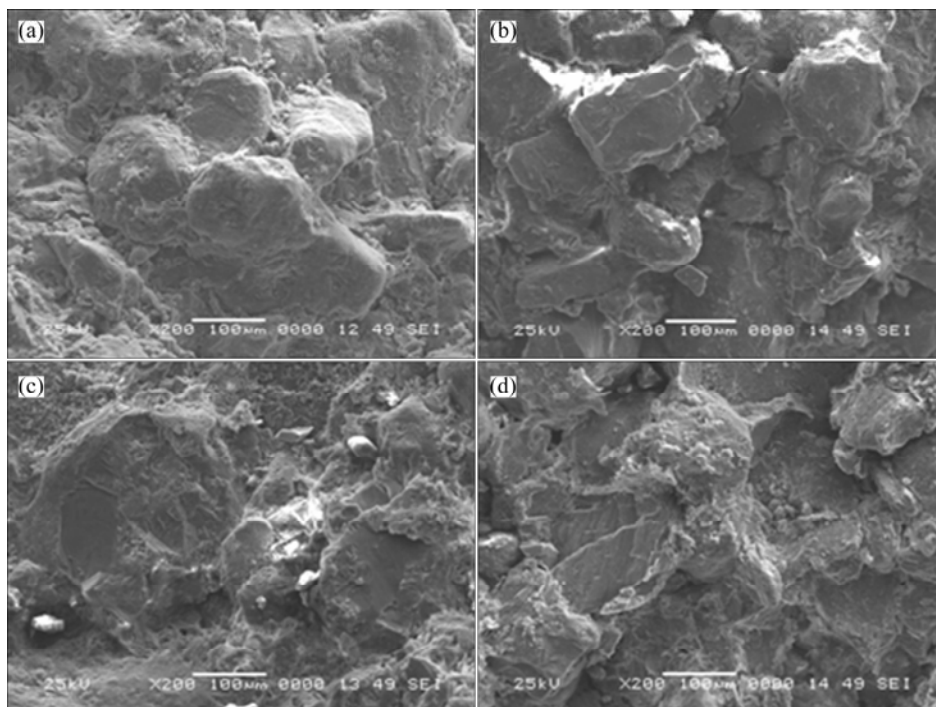


**Fig. 11** Fracture morphologies of red sandstone at different confining pressures: (a) Specimen M1 (intergranular fracture); (b) Specimen M2 (transgranular and intergranular fracture); (c) Specimen T1 (transgranular fracture); (d) Specimen M3 (transgranular fracture)

## 4 Conclusions

1) Traditional boundary collocation method is only suitable for calculating stress intensity factor of the

cracked specimen without any force on its crack surface. By successfully introducing an additional constant stress function into the boundary collocation method, a calculation formula of THM coupling stress intensity factor of the cracked specimen (with hydraulic pressure

applied on its crack surface) was firstly derived, which is very important both for improving classical fracture mechanics theory and for providing evidence for fracture prediction, safety assessment and cracking-arrest design in THM coupling rock engineering.

2) The maximum THM coupling stress intensity factors can be determined by substituting the maximum axial load measured by self-designed THM coupling fracture test into the newly-derived THM coupling stress intensity factor formula. THM coupling fracture modes (including tensile, shear and mixed fracture mode) can be predicted based on a new fracture criterion of stress intensity factor ratio.

3) SEM analyses of THM coupling fractured surface indicated that the higher the temperature and hydraulic pressure are and the lower the confining pressure is, the more easily the intergranular (tension) fracture occurs. The transgranular (shear) fracture occurs in the opposite case and the mixed-mode fracture occurs in the middle case. The tested THM coupling fracture mechanisms are in good agreement with the predicted THM coupling fracture modes, which can verify correction of the newly-derived THM coupling stress intensity factor formula.

## References

- [1] JING L, TSANG C F, STEPHANSSON O. DECOVALEX—An international co-operative research project on mathematical models of coupled THM processes for safety analysis of radioactive waste Repositories [J]. *International Journal of Rock Mechanics and Mining Sciences*, 1995, 32(5): 389–398.
- [2] HUDSON J A, STEPHANSSON O, ANDERSSON J, TSANG C F, JING L. Coupled T–H–M issues relating to radioactive waste repository design and performance [J]. *International Journal of Rock Mechanics and Mining Sciences*, 2001, 38(1): 143–161.
- [3] RUTQVIST J, CHIJIMATSU M, JING L, MILLARD A, NGUYEN T S, REJEB A, SUGITA Y, TSANG C F. A numerical study of THM effects on the near-field safety of a hypothetical nuclear waste repository-BMT1 of the DECOVALEX III project. Part 3: Effects of THM coupling in sparsely fractured rocks [J]. *International Journal of Rock Mechanics and Mining Sciences*, 2005, 42(5–6): 745–755.
- [4] XIE Hai-feng, RAO Qiu-hua, XIE Qiang, LI Zong-yu, WANG Zhi. Plane shear (Mode II) fracture experiment analysis of brittle rock at high temperature [J]. *The Chinese Journal of Nonferrous Metals*, 2008, 15(s1): 402–405. (in Chinese)
- [5] CHAN T, KHAIR K, JING L, AHOLA M, NOORISHAD J, VUILLOD E. International comparison of coupled thermo-hydro-mechanical models of a multiple-fracture bench mark problem: DECOVALEX phase I, bench mark test 2 [J]. *International Journal of Rock Mechanics and Mining Sciences & Geomechanics Abstracts*, 1995, 32(5): 435–452.
- [6] SHAHANI A R, NABAVI S M. Closed form stress intensity factors for a semi-elliptical crack in a thick-walled cylinder under thermal stress [J]. *International Journal of Fatigue*, 2006, 28(8): 926–933.
- [7] NABAVI S M, GHAJAR R. Analysis of thermal stress intensity factors for cracked cylinders using weight function method [J]. *International Journal of Engineering Science*, 2010, 48(12): 1811–1823.
- [8] JOHNSON J, QU J. An interaction integral method for computing mixed mode stress intensity factors for curved bimaterial interface cracks in non-uniform temperature fields [J]. *Engineering Fracture Mechanics*, 2007, 74(14): 2282–2291.
- [9] LIU Jun-yu, LIN Gao. Effect of the water pressure inside the crack on the fracture behavior of concrete gravity dam [D]. Dalian: Dalian University of Technology, 2008. (in Chinese)
- [10] YEW C H, LIU G F. The fracture tip and critical stress intensity factor of a hydraulically induced fracture [J]. *SPE Production and Facilities*, 1993, 8(3): 171–177.
- [11] LI Xi-bing, HE Xian-qun, CHEN Hong-jiang. Crack initiation characteristics of opening-mode crack embedded in rock-like material under seepage pressure [J]. *Chinese Journal of Rock Mechanics and Engineering*, 2012, 31(7): 1317–1324. (in Chinese)
- [12] ZHAO Yan-lin, CAO Ping, WEN You-dao, YANG Hui, LI Jiang-teng. Damage fracture failure mechanism of compressive-shear rock cracks under seepage pressure [J]. *Journal of Central South University: Science and Technology*, 2008, 39(4): 838–844. (in Chinese)
- [13] HUANG K, GHASSEMI A. Modeling 3d hydraulic fracture propagation and thermal fracture using virtual multidimensional internal bonds [J]. *Geothermal Reservoir Engineering*, 2012, 18(1): 311–320.
- [14] MOHAMMADREZA J. Thermo-hydro-mechanical behavior of conductive fractures using a hybrid finite difference-displacement discontinuity method [D]. Waterloo: University of Waterloo, 2013.
- [15] RAO Q H, SUN Z Q, STEPHANSSON O, LI C L, STILLBORG B. Shear fracture (Mode II) of brittle rock [J]. *International Journal of Rock Mechanics and Mining Sciences*. 2003, 40(3): 355–375.

# 脆性岩石热–水–力耦合应力强度因子计算

李鹏<sup>1</sup>, 饶秋华<sup>1</sup>, 李卓<sup>1</sup>, 敬静<sup>2</sup>

1. 中南大学 土木工程学院, 长沙 410075; 2. 中南大学 资源与安全工程学院, 长沙 410083

**摘要:** 采用边界配置法并引入附加的常应力函数, 成功地推导出岩石热–水–力(THM)耦合条件下含裂纹试件(裂纹面有水压作用)的裂尖应力强度因子计算公式。利用自行设计的 THM 耦合断裂试验, 测定脆性岩石 THM 耦合断裂的最大轴压, 并依据新推导的公式和新型应力强度因子比断裂准则预测脆性岩石 THM 耦合断裂模式。岩石 THM 耦合断口的形貌特征分析结果表明: 温度、水压越高, 围压越低, 沿晶(拉伸)断裂越容易发生; 反之, 则穿晶(剪切)断裂更容易发生; 而介于两者中间时, 则复合型断裂更容易发生。测得的 THM 耦合断裂机理与预测的 THM 耦合断裂模式结论一致, 从而验证了推导出的 THM 耦合应力强度因子计算公式的正确性。

**关键词:** 应力强度因子; 热–水–力耦合; 边界配置法; 断裂机理; 脆性岩石

(Edited by Sai-qian YUAN)